13th ewtec 2019
Proceedings of the 13th European Wave and Tidal Energy Conference 1-6 Sept 2019, Naples, Italy

# Three-Dimensional Unsteady Hydrodynamic Modelling of Tidal Turbines

Amanda S. M. Smyth, and Anna M. Young

***Abstract*—Predicting the response of a tidal turbine to unsteady inflow conditions is a challenge for turbine designers, with consequences for fatigue life and manufacturing costs. The unsteady load models currently used are all based on 2D strip-theory methods. However, the assumption of locally 2D flow is not likely to apply to tidal turbines, and the effect of 3D geometry on the unsteady response is not widely known. This study uses a combination of time-stepping and frequency-domain vortex lattice models, together with URANS simulations, to show the effects of 3D geometry on the unsteady load response of a tidal turbine. The effects of steady-state wake rollup and of unsteady distortion of the wake by the inflow are quantified in terms of their impact on both the mean and the unsteady load. Comparisons to predictions from classical 2D aerofoil theory show significant differences between 2D and 3D modelling, especially for torque predictions. The frequency-domain inviscid vortex lattice model agrees well with the URANS result, suggesting that it is an appropriate tool for unsteady turbine hydrodynamic analysis.**

***Index Terms*—3D modelling, gust response, unsteady aerodynamic theory, URANS, vortex lattice model.**

## I. Introduction

THE nature of tidal channel flow presents unique challenges to device designers, due to the significant presence of unsteady flow and turbulence [1]. This unsteady flow affects power output, and generates time-varying blade loading, which leads to fatigue damage and integrity issues. The standard methods used to predict unsteady loading are based on those employed by the wind industry. However, the problem of unsteady aerodynamic loading is of much larger consequence for tidal turbines due to the high density of water [2]. Given this difference between wind and tidal turbines, it is necessary to evaluate the models used for unsteady load prediction, and to examine the assumptions made. Recent studies have suggested that the level of uncertainty in current unsteady load models could result in an order of magnitude error in fatigue life estimates [3], leading to over-engineered designs or premature failure. Improving the modelling of unsteady loads will therefore reduce costs and increase reliability of tidal turbines.

Paper ID 1522, Tidal Hydrodynamic Modelling. This work has been performed using resources provided by the Cambridge Tier-2 system operated by the University of Cambridge Research Computing Service (http://www.hpc.cam.ac.uk) funded by EPSRC Tier-2 capital grant EP/P020259/1.

A. S. M. Smyth is a PhD student at the Whittle Laboratory at Cambridge University, 1 JJ Thomson Avenue, CB3 0DY Cambridge, U.K. (e-mail: asmms2@cam.ac.uk).

A. M. Young was previously at the University of Cambridge. She is now a Lecturer at the University of Bath, Claverton Down Road, BA2 7AY Bath, U.K. (e-mail: amy32@bath.ac.uk).

Turbine modelling for preliminary design is commonly based on Blade Element Momentum Theory (BEMT). In this strip-theory method, the blade is divided into annular 2D sections which are assumed to be independent of each other [4]. Empirical and semi-empirical models are used to correct for the effect of three-dimensional flow on the steady performance. In order to estimate unsteady blade loading, the industry-standard design software TidalBladed uses "classical" unsteady aerofoil theory to estimate the variation in load at each blade section [5]. The classical theory assumes that the flow can be approximated as inviscid flow over a 2D flat plate at zero mean angle of attack, which allows the derivation of analytical unsteady transfer functions (see [6] for a summary). These unsteady transfer functions give the load variation for a given unsteady inflow velocity as a function of the quasi-steady 2D lift coefficient, and are readily applicable to BEMT methods. Examples of transfer functions include the Theodorsen function [7] for uniform gusts and the Sears function [8] for sinusoidal gusts.

Other commonly used methods for transient load calculations include dynamic inflow models, which in their simplest forms provide estimates only for the added mass effects caused by the transient flow. More advanced dynamic inflow models have been developed for helicopter rotor applications [9], and have been adapted for use in wind turbines [10]. All classical and dynamic inflow methods are based on the assumption of localised 2D flow, with no interaction between different turbine annulus sections. This assumption of 2D flow has little backing in literature. It is unlikely to hold in the case of tidal turbine blades (which generally have low aspect ratios and are highly tapered), and there is virtually no knowledge of the effects of 3D geometry on unsteady blade loading. The purpose of this paper is to investigate whether the assumption of localised 2D flow holds for unsteady load calculations, and to find the limits of applicability of 2D unsteady flow theory to a 3D turbine geometry.

Recent studies of unsteady flow effects on wind and tidal turbines have primarily focused on dynamic stall [11] [12] [13], and on the effect of waves [14] [15]. Experimental studies of unsteady turbine response have provided valuable data (such as: [14] [16] [17] [18]) but there is no robust insight into the physical mechanisms of unsteady loading.

McNae studied the unsteady response of a full 3D turbine geometry using a time-stepping vortex panel method [17]. Whelan carried out experimental tests of oscillatory turbine forcing [18]. Both these studies found that dynamic inflow models used with BEMT could predict the right loading trends, but not the right load magnitude. The findings of McNae and Whelan suggest that 2D BEMT models are failing to capture important flow physics.

In other fields, some work has been done on quantifying 3D unsteady effects. Kinnas [19] used an unsteady time-domain vortex panel method in 3D to estimate the unsteady loads experienced by boat propellers interacting with the wakes of the boats. Namba [20] and Schulten [21] both developed semi-analytical models for the unsteady response of ducted fan blades, capable of analysing subsonic, transonic and supersonic flows. Their work has been used for the validation of a number of 3D Euler solvers for internal flow turbomachinery [22] [23]. In general, studies that have set out to determine the accuracy of 2D strip-theory models compared to fully 3D models have found the strip theory lacking in accuracy, especially in the region near the blade tip [22] [24].

In a recent study by Smyth et al [25], the major driver for 3D unsteady load response was found to be the combined effect of the spanwise and streamwise components of unsteady wake vorticity. The presence of an unsteady streamwise wake, which is inherent to 3D geometry, causes significant deviation from 2D predictions across the blade span. The study was conducted using a frequency-domain vortex lattice model (VLM), and so the impact of viscous and second order effects such as wake rollup and distortion were not included.

This paper presents the results of a parametric study of the unsteady load response of a tidal turbine, including the effects of wake rollup, wake distortion and viscosity. The study was performed using Unsteady Reynolds-Averaged Navier-Stokes (URANS) simulations, and vortex lattice model calculations in two configurations: frequency-domain and time-domain. The results are compared to classical 2D unsteady aerofoil theory. For the purpose of parameterisation, the unsteady flow is modelled as harmonic variations in the flow field. The cases considered are uniform flow oscillating in the axial direction, and axial flow varying sinusoidally in the circumferential plane. Both of these idealised gusts are locally 2D, with no variation along the blade span. As such, the impact of 3D geometry is isolated.

The results show that the 3D vortex lattice method is able to capture the loading trends and magnitudes seen in the URANS CFD. The effect of including wake rollup in the vortex lattice model is to lower the average (steady-state) loads, and to intensify returning wake interaction effects. The URANS results show that viscous stall effects only have a small impact on the unsteady load amplitude for the moderate-sized gusts considered in this paper. This suggests that the low-order vortex lattice code is an appropriate tool for predicting the unsteady loading on tidal turbines.

## II. Unsteady aerodynamics and classical aerofoil theory

Classical unsteady aerofoil theory assumes inviscid, incompressible flow about a 2D flat plate at zero mean angle of attack. The interaction of unsteady flow with a lifting surface results in two physical effects that generate lift response: the added mass and the unsteady wake [6]. The added mass results from the fluid around the aerofoil being accelerated and imparting a resultant force on the aerofoil (which is proportional to the rate of change of the aerofoil circulation with respect to time). If the unsteady flow occurs with high frequency, this added mass force may become very large. The unsteady wake is necessary to satisfy Kelvin's theorem of constant circulation in the flow. As the aerofoil interacts with the unsteady flow, its circulation changes and therefore a vortex of equal and opposite strength must be shed. In a harmonically varying flow, vortices are therefore being shed continuously, creating the unsteady wake. This wake induces a downwash velocity on the aerofoil, imparting unsteady aerodynamic damping on the aerofoil lift. This coupling between the unsteady wake and the aerofoil drives the unsteady load response.

In classical aerofoil theory the 2D unsteady lift can be obtained using unsteady transfer functions, which modify the lift coefficient. For the purpose of comparison between 2D and 3D predictions, this paper uses the 2D unsteady transfer functions derived by Theodorsen [7], Sears [8] and Loewy [26]. The Theodorsen function is used for harmonic flow variation acting uniformly along the chord. The Loewy function acts as a modifier to the Theodorsen function to account for the returning wake effects, which is necessary for rotating aerofoils. However, a previous study of the turbine used in this work showed that, for this particular geometry, the estimate from the Loewy function did not differ much from that of the Theodorsen function [25]. The Sears function is applicable to harmonic flow with sinusoidal spatial variation. Unlike the Theodorsen function, the Sears function has no associated modifier for the returning wake.

The harmonic transfer functions take the reduced frequency, $k$, as an input variable. This is a measure of the number of chord lengths a particle travels per gust wavelength. The unsteady lift coefficient of a 2D aerofoil subjected to a gust acting uniformly across the chord with frequency $\omega$ is obtained by:

$$Cl' = [2\pi C(k/2) - i\pi k/2]\hat{\alpha}e^{i\omega t} \quad (1)$$

with the reduced frequency given by:

$$k = \frac{\omega * \text{chord}}{U} \quad (2)$$

TABLE I
FORMS OF THE INFLUENCE MATRIX A USED IN THE VORTEX LATTICE MODEL

(a) Frequency-domain:

$$A = \begin{bmatrix} a_{1,1} & a_{1,2} & \dots & a_{1,n}+b_{1,1} & a_{1,n+1} & a_{1,n+2} & \dots & a_{1,N}+b_{1,m} \\ a_{2,1} & a_{2,2} & \dots & a_{1,n}+b_{2,1} & a_{2,n+1} & a_{2,n+2} & \dots & a_{1,N}+b_{2,m} \\ \vdots & \vdots & \ddots & \vdots & \vdots & \vdots & \ddots & \vdots \\ a_{N,1} & a_{N,2} & \dots & a_{N,n}+b_{N,1} & a_{N,n+1} & a_{N,n+2} & \dots & a_{N,N}+b_{N,m} \end{bmatrix} \begin{bmatrix} \hat{\Gamma}_1 \\ \hat{\Gamma}_2 \\ \vdots \\ \hat{\Gamma}_N \end{bmatrix} = - \begin{bmatrix} (\hat{u}_{gust})_1 \\ (\hat{u}_{gust})_2 \\ \vdots \\ (\hat{u}_{gust})_N \end{bmatrix}$$

(b) Time-domain:

$$A = \begin{bmatrix} a_{1,1} & a_{1,2} & \dots & a_{1,n} & a_{1,n+1} & a_{1,n+2} & \dots & a_{1,N} \\ a_{2,1} & a_{2,2} & \dots & a_{1,n} & a_{2,n+1} & a_{2,n+2} & \dots & a_{1,N} \\ \vdots & \vdots & \ddots & \vdots & \vdots & \vdots & \ddots & \vdots \\ a_{N,1} & a_{N,2} & \dots & a_{N,n} & a_{N,n+1} & a_{N,n+2} & \dots & a_{N,N} \end{bmatrix} \begin{bmatrix} \Gamma_1 \\ \Gamma_2 \\ \vdots \\ \Gamma_N \end{bmatrix} = - \begin{bmatrix} (u_\infty + u_{wake} + u_{gust})_1 \\ (u_\infty + u_{wake} + u_{gust})_2 \\ \vdots \\ (u_\infty + u_{wake} + u_{gust})_N \end{bmatrix}$$

$\hat{\alpha}$ is the amplitude of the oscillating angle of attack. The function $C(k/2)$ is the Theodorsen function, which uses the reduced frequency to determine the lift modifier, due to the aerodynamic damping caused by the unsteady wake and the added mass effect. Theodorsen's function is expressed in terms of Hankel functions, using the reduced frequency as a parameter. The exact form of the Theodorsen function in terms of Bessel and Hankel functions can be found in textbooks, such as Leishman's [6]. For sinusoidal gusts, the Sears function developed by von Karman and Sears [8] gives the lift coefficient as:

$$Cl' = 2\pi S(k/2)\hat{\alpha}e^{i\omega t} \tag{3}$$

The function $S(k/2)$ is the Sears function. At small reduced frequencies both (1) and (3) reduce to the 2D lift coefficient for a flat plate, $2\pi\hat{\alpha}$.

While the Theodorsen function is the more commonly used function for estimating unsteady loads on tidal turbines, sinusoidal gusts have been shown to be more representative of ocean turbulence [27]. Evaluating the response of a turbine to sinusoidal gusts requires the Sears function. In this study, the accuracy of both functions is evaluated on a 3D geometry.

## III. THE UNSTEADY VORTEX LATTICE MODEL

### A. Method

The unsteady vortex lattice model captures the inviscid unsteady load with the same accuracy as classical aerodynamic theory, while also allowing for camber, finite blade span and spanwise geometry variation if used in the 3D configuration. The model used in this study is based on those by Katz and Plotkin [28] and has been modified to allow for frequency-domain calculations. An illustration of the basic 3D model is shown in Fig. 1. The aerofoil is divided into panels, each with an associated vortex ring (shown in blue in Fig. 1) and a collocation point (red dots in Fig. 1). The vortex rings give the aerofoil its circulation, and the boundary conditions and forces are evaluated at each collocation point. The Kutta condition is inherently satisfied by the placement of the vortex ring at the quarter-chord of each panel, and the collocation point at three-quarter chord. The wake is formed by allowing the trailing edge vortex ring to be shed into the freestream at each time step. This vortex ring method does not model blade thickness, so blade thickness effects are not studied in this project. However, the thickness has only marginal effect on the total blade loads in inviscid modelling, so this will not affect the accuracy of the model.

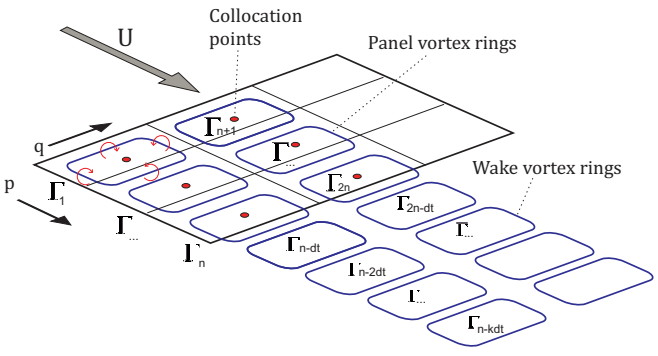


Fig. 1. Structure of the 3D vortex lattice model.

To find the circulation of each panel, Neumann's boundary condition of zero flow normal to the surface is applied at each collocation point. The Biot-Savart law is used to calculate the velocity induced by each vortex ring on each collocation point. Adding the freestream velocity, $\boldsymbol{U}_\infty + \boldsymbol{u}_{gust}$, and the wake-induced velocity, $\boldsymbol{u}_{wake}$, the resulting matrix equation has the following form:

$$(\mathbf{A\Gamma} + \boldsymbol{U}_\infty + \boldsymbol{u}_{gust} + \boldsymbol{u}_{wake}).\mathbf{n} = 0 \tag{4}$$

The vector $\mathbf{\Gamma}$ gives the unknown circulations of each aerofoil vortex ring. The matrix $\boldsymbol{A}$ is the influence matrix, which represents the shape of the aerofoil and applies the Biot-Savart law. The Biot-Savart law for the velocity induced by a vortex line with strength $\Gamma$ is given by:

$$\mathbf{v} = \frac{\Gamma}{4\pi}\frac{\boldsymbol{r_1}\times\boldsymbol{r}_2}{|\boldsymbol{r}_1\times\boldsymbol{r}_2|^2}(\boldsymbol{r}_0\cdot(\frac{\boldsymbol{r}_1}{|\boldsymbol{r}_1|}-\frac{\boldsymbol{r}_2}{|\boldsymbol{r}_2|})) = \Gamma\boldsymbol{a} \tag{5}$$

In this notation, for the velocity induced at point $\boldsymbol{p}$ by a vortex line between points $\boldsymbol{p}_1$ and $\boldsymbol{p}_2$, the vectors $\boldsymbol{r}_1$ and $\boldsymbol{r}_2$ are given by $\boldsymbol{p}_1 - \boldsymbol{p}$ and $\boldsymbol{p}_2 - \boldsymbol{p}$, respectively. The vector $\boldsymbol{r}_0$ is given by $\boldsymbol{p}_1 - \boldsymbol{p}_2$.

Two versions of the vortex lattice model were used for this study: one using frequency-domain modelling and one using time-domain modelling. Modelling in the frequency domain greatly increases the speed of

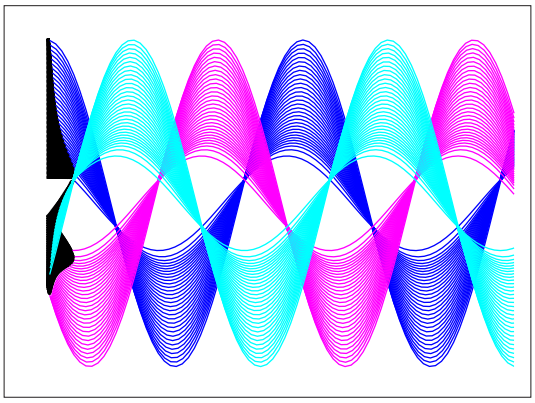

(a) Prescribed wake, frequency-domain VLM

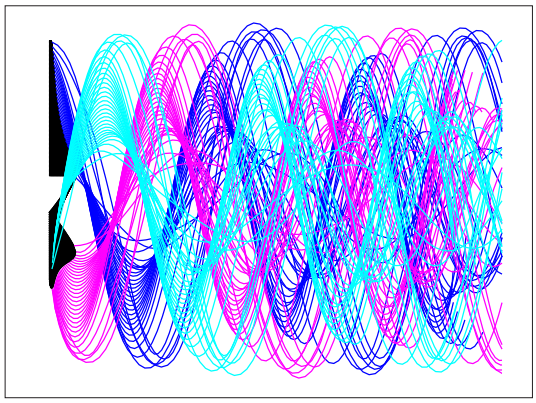

(b) Free wake, time-domain VLM

Fig. 2. Vortex lattice model with (a) prescribed wake based on the steady freestream flow, and (b) free-wake model.

the simulations. A time-stepping simulation may take hours while an equivalent harmonic simulation takes minutes. The frequency-domain model does, however, require a prescribed wake shape. The simplest and most common method is to assume that the wake vortices leave the trailing edge with the steady freestream flow speed. However, in reality, the wake vortices interact with each other, leading to additional distortion of the wake. Fig. 2 shows the difference between a standard prescribed wake used in the frequency domain (Fig. 2a), and a free wake obtained from a time-stepping code (Fig. 2b). The two main distortion effects seen in Fig. 2b are wake rollup near the tip and hub, and an overall deceleration in the wake. In this work, the vortex lattice model will be studied in both the frequency and the time domain, in order to quantify the impact of the wake shape on the unsteady load generation.

### B. Frequency-domain calculations

The basic version of the vortex lattice model used in this project is the frequency-domain version with a prescribed wake, with the assumption that the wake propagates with the steady freestream velocity (as in Fig. 2a). In the frequency domain, all unsteady variables are assumed to vary harmonically with the form:

$$\Gamma(t) = \hat{\Gamma} e^{i\omega t} \tag{6}$$

The system given by equation (4) can be solved for the circulation amplitude $\hat{\Gamma}$, which when multiplied by $e^{i\omega t}$ gives the response at any time. The circulation of the wake vortices can be inferred by noting that the trailing edge circulation varies harmonically, and so the circulation strength of a given wake vortex is the same as that of the trailing edge panel at the time the vortex was shed. This allows the wake-induced velocity to be calculated, retaining the notation in the Biot-Savart law in (5) and the wake numbering in Fig. 1:

$$\boldsymbol{u}_{wake} = \Gamma_{TE} \sum_{k=1}^{\infty} \boldsymbol{a} e^{-\omega * k * dt} = \Gamma_{TE} \boldsymbol{b} \tag{7}$$

Using this expression for the wake velocity, the influence matrix $\boldsymbol{A}$ can be created, and equation (4) can therefore be solved for the unsteady circulation amplitude $\hat{\boldsymbol{\Gamma}}$. The time step $dt$ used in (7) is not used for explicit time-stepping, but is chosen as an input parameter determining the resolution of the wake. Sufficient wake resolution is vital for accurate unsteady calculations. The accuracy condition found in this project was that the length of the wake vortex in the direction indicated by "p" in Fig. 1 had to be smaller than the length of the aerofoil panels. Throughout this work the time step $dt$ was chosen so that the wake vortex rings were no more than half the aerofoil panel length.

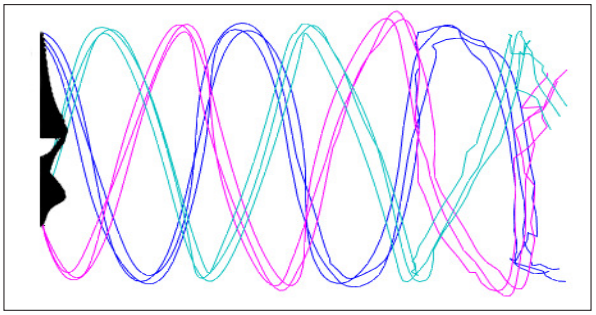

(a) Vortex lattice model

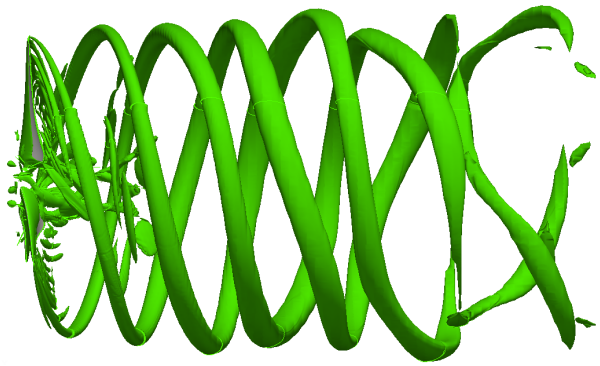

(b) URANS

Fig. 3. Illustration of the wake distorted by a uniform unsteady gust with mid-span reduced frequency 0.75. (a) shows the wake of the time stepping vortex lattice model when using equation (14). For clarity, only the three outermost wake vortices of each blade are shown. (b) shows the q-criterion surface contours of a URANS case with the same gust applied. Data from a third of the annulus has been extrapolated to obtain the full-annulus field.

The form of the frequency-domain influence matrix can be found in Table I, equation (a). The matrix size is $N \times N$, where $N$ is given by multiplying the number of chordwise panels $n$ by the number of panels across the span $m$. The notation $i$ represents the collocation point where the Biot-Savart law is evaluated. The notation $j$ represents the vortex ring acting on the collocation point. For simplicity of notation, the vectors $\boldsymbol{a}$ and $\boldsymbol{b}$ from equations (5) and (7) are written in Table I as the dot products with the panel normal vector.

The circulation vector $\hat{\boldsymbol{\Gamma}}$ is obtained by inverting the matrix equation in (4), and is then used to obtain the lift force from the vector form of the Kutta-Joukowski theorem:

$$\boldsymbol{F} = \rho(\boldsymbol{U} \times \boldsymbol{\Gamma}) = \rho[(\boldsymbol{u}_{rel} + \boldsymbol{u}_{gust} + \boldsymbol{u}_{wake}) \times \boldsymbol{\Gamma}] \quad (8)$$

The velocity vector $\boldsymbol{u}_{rel}$ represents the relative velocity given by:

$$\boldsymbol{u}_{rel} = \boldsymbol{U}_\infty + \boldsymbol{u}_{rot} = \boldsymbol{U}_\infty + TSR|\boldsymbol{U}_\infty|\boldsymbol{e}_\theta \quad (9)$$

where TSR denotes the tip-speed ratio, and $\boldsymbol{e}_\theta$ is the tangential unit vector.

Further details of the frequency-domain vortex lattice model and its validation against steady 3D and unsteady 2D cases can be found in [25].

### C. Time-domain calculations

In the time-domain the influence matrix is solved at each discrete time step, which simplifies the calculations but is substantially more time-consuming. The wake-induced velocity is calculated using (5) and the wake vortex circulation calculated in the previous time step. The change to the influence matrix $\boldsymbol{A}$ in (4) is given in Table I, equation (b).The aerofoil circulation vector $\Gamma$ is obtained and used to calculate the time-history of unsteady loading using (8). The circulations of the new shed wake vortices are found and stored for use in the next time step.

In the time stepping method it is possible to calculate the positions of the wake vortices as a summation of influence by the steady freestream, the unsteady gust, and all the other wake vortices. In order to quantify the relative importance of each of these influences on the unsteady response, solutions will be shown with different terms included and excluded. The movement of each wake vortex at each time step is obtained by:

$$d\boldsymbol{l} = dt.\boldsymbol{u} \quad (10)$$

The velocity vector $\boldsymbol{u}$ can be calculated by considering up to four different combinations of influences:

$$\boldsymbol{u} = \boldsymbol{U}_\infty + \boldsymbol{u}_{rot} \quad (11)$$

$$\boldsymbol{u} = \boldsymbol{U}_\infty + \boldsymbol{u}_{rot} + \boldsymbol{u}_{wake} \quad (12)$$

$$\boldsymbol{u} = \boldsymbol{U}_\infty + \boldsymbol{u}_{rot} + \boldsymbol{u}_{gust} \quad (13)$$

$$\boldsymbol{u} = \boldsymbol{U}_\infty + \boldsymbol{u}_{rot} + \boldsymbol{u}_{wake} + \boldsymbol{u}_{gust} \quad (14)$$

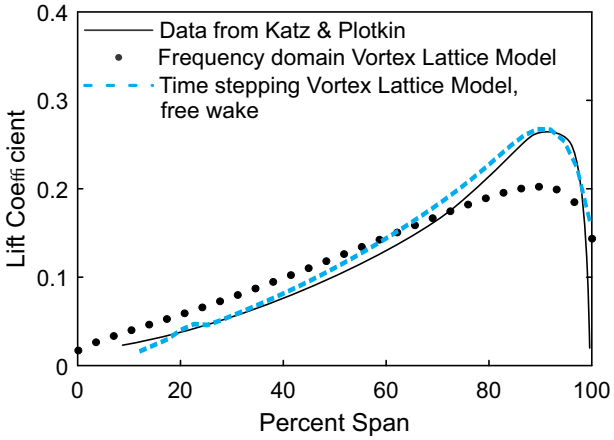


Fig. 4. Results from Katz and Plotkin [28], compared to those obtained by the frequency domain code described in section III-B and the time stepping code described in section III-C.

Note that since the calculations are carried out in the relative frame, the rotational velocity $\boldsymbol{u}_{rot}$ must always be included. The velocity vector as given by (11) results in the same wake shape as used in the basic frequency-domain model outlined in the previous section (resulting in the wake in Fig. 2a). If (11) was used to generate the wake in the time stepping model, the results were identical to those of the frequency-domain model. The vector given by (12) includes the effects of the surrounding wake vortices (resulting in the wake in Fig. 2b in steady flow conditions), which we will refer to as "wake rollup". The vector given by using (13) includes the distorting effect of the unsteady gust. Finally, the vector given by (14) includes the combination of both wake rollup and gust distortion. As an example, Fig. 3 shows the wake shape generated by (14) for a uniform gust interacting with the turbine at mid-span reduced frequency of about 0.75. The wake of a URANS simulation of the same gust is shown for comparison.

Katz and Plotkin [28] use an experimental test by Caradonna and Tung [29] to validate their time stepping panel method. The experiment is of a two-bladed rotor with a NACA 0012 aerofoil (modelled as a flat plate in the VLM). The results from Katz and Plotkin are shown in Fig. 4, along with results obtained from the vortex lattice models in the frequency-domain (using (11) to obtain the wake) and time-domain (using (12)). The distinctive features of the prescribed wake as opposed to the free wake calculations can be seen: the prescribed wake predicts a more linear variation in lift along the span, while the free wake model predicts a nonlinear increase and is in better agreement with the experimental data.

### D. Steady wake correction in the frequency-domain

To improve the accuracy of the frequency-domain model with a minimal increase in computational time, a steady correction to the wake shape was implemented. A wake is allowed to develop in steady flow conditions in the time-stepping code described in section III-C, using (12) to generate the wake. The

resulting steady wake is then used as an input to the unsteady frequency-domain calculations described in III-B. The increase in computational time for this correction is minimal, as the wake only needs to be generated once for a given TSR. The steady model also has less stringent requirements on the wake resolution, which speeds up the calculations. This steady wake correction allows rapid evaluation of wake rollup effects on unsteady load across a range of unsteady flow frequencies. The results of this correction will be shown in section V-C.

## IV. URANS SIMULATIONS

### E. Geometry, mesh and solver

The geometry used in this study is a 3-bladed model tidal turbine (see Fig. 5). It has been used extensively in experimental studies of steady and unsteady turbine performance. The turbine is 700 mm in diameter, with a rated TSR of 4. The mid-span Reynolds number at rated TSR is in the order of 130,000. Further details of turbine design and performance can be found in [14].

The CFD simulations are performed with an Unsteady Reynolds-Averaged Navier Stokes (URANS) solver, using the open source CFD software OpenFOAM [31]. The solver "pimpleDyMFoam" was used. The PIMPLE algorithm used in this solver is a combination of the PISO (Pressure Implicit with Splitting of Operator) and SIMPLE (Semi-Implicit Method for Pressure-Linked Equations) algorithms. The algorithm allows stable transient simulations at Courant numbers much larger than 1, by applying relaxation factors to each time-step until a certain convergence criterion is met, before allowing the time-step to complete with no applied relaxation factors.

The letters "DyM" in the OpenFOAM solver stand for "Dynamic Mesh", meaning that the solver has moving mesh capability. For the transient CFD simulations, the whole mesh was rotated at 11.4 rad/s (TSR 4 for 1 m/s axial inlet flow speed). For the steady simulations, the solver "SRFSimpleFoam" was used, which solves the field in the rotating reference frame.

All meshes are structured and were created using the meshing software Pointwise. A single blade in a third of an annulus was modelled, using periodic boundary conditions on the circumferential boundaries in order to capture the returning wake effects from the remaining two blades (see Fig. 7a). The turbine hub and nacelle are not modelled and the centre and far-field boundaries are modelled as inviscid walls. A mesh sensitivity study was carried out to determine the appropriate inlet and exit lengths of the domain, which resulted in mesh dimensions of 2 turbine diameters upstream and 4 turbine diameters downstream of the blade-centred block (see Fig. 6), as a compromise between performance and computational cost. The radial domain distance is 2.8 turbine diameters, chosen based on the depth of the test tank at Ifremer in Bologne, France, where the experimental testing of the model turbine was performed.

The required chordwise aerofoil resolution and y+ value were determined through 2D tests of a blade section. The Cp distributions and lift characteristic were compared to results from MSES, a coupled potential and boundary layer solver which is

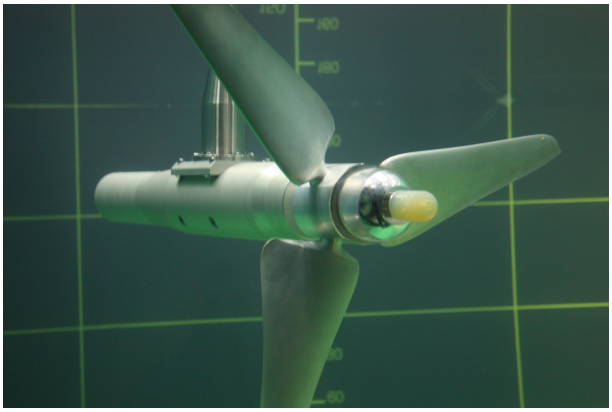

(a) Experiment (picture from [30])

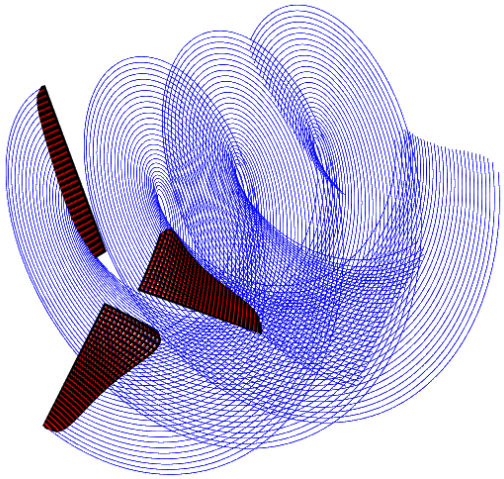

(b) Vortex lattice model

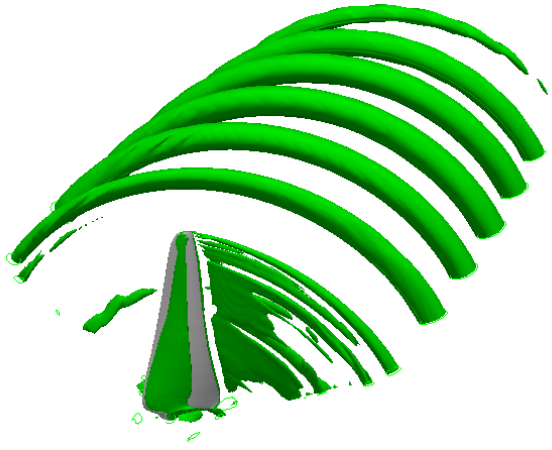

(c) URANS

Fig. 5. The turbine: (a) experimental test at Ifremer, France, (b) vortex lattice model, (c) CFD simulation of a third of the annulus, showing vorticity contours identified with the q-criterion.

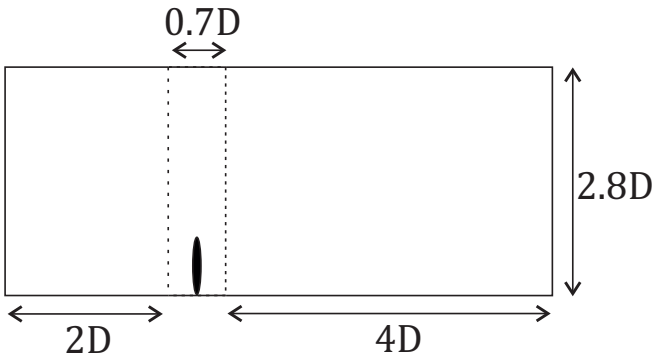


Fig. 6. Boundaries of the computational domain used for URANS simulations.

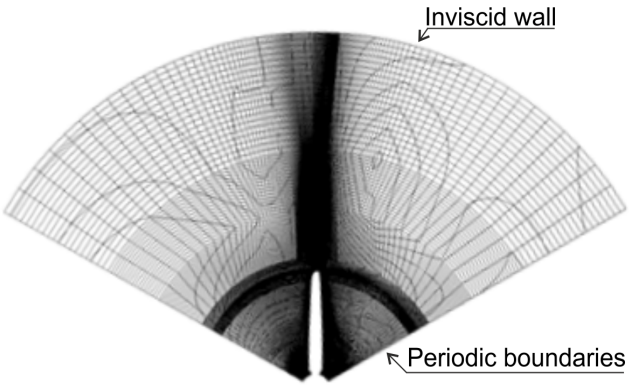


(a) Axial cross-section of mesh

(b) Blade surface mesh

Fig. 7. Deatil of the structured mesh used for steady and unsteady RANS simulations.

extensively validated against experimental studies of NACA blade profiles [32]. A y+ value of 60 with wall functions gave a good agreement with the MSES pressure coefficient distributions in pre-stall conditions and was found to be a good compromise between accuracy and computational cost. Chordwise resolutions of 100 and 140 cells on the pressure and suction surfaces were tested and were shown to give similar results in terms of both steady and unsteady lift response. In the final 3D mesh the pressure and suction surfaces each have 110 cells. The trailing edge is round and has 12 cells. Fig. 7a shows the axial cross-section of the mesh, and Fig. 7b shows detail of the blade surface mesh. The mesh is refined in the region of the tip vortex, and near the tip and hub of the blade. The total cell count is approximately 17 million.

The turbulence model used for this study was $k\omega - SST$, which has been found in many studies to offer the closest agreement with experimental data for tidal turbine performance. The relatively large thickness of the aerofoil used means that it fails via trailing edge separation, which creates a gradual loss of lift at high angles of attack. This gradual trailing edge stall was not captured well by the standard solver schemes used in OpenFOAM. Fig. 8 shows the steady 2D lift performance of the aerofoil, showing the prediction by MSES (black line) and OpenFOAM using default solver discretisation schemes (blue circles) and high-order schemes (red circles). Using the default settings, the flow remained attached at higher incidence than the MSES prediction. It was found that for a high resolution 2D mesh, higher-order schemes could capture the angle of attack at which stall began, but not the lift curve beyond this point: the CFD predicted a much more abrupt loss of lift than MSES. For the final 3D simulations, the standard OpenFOAM solver schemes were chosen, as they were more stable. As such, it is important to know that the 3D URANS calculations are likely to predict flow that remains attached at higher incidences than is realistic.

### F. *Generation of unsteady flow*

The unsteady flow was generated by varying the inlet velocity. Two classes of harmonic inflow were applied: axially uniform flow variation and annular-sinusoidal flow variation, as illustrated in Fig. 9. To generate the axially uniform flow variation (Fig. 9a) the inlet velocity was uniformly oscillated as a function of time across the whole inlet. This created a pressure wave that propagated rapidly through the computational domain without dissipating. There was sufficient distance between the domain outlet and the turbine to ensure that pressure wave reflection from the outlet did not affect the turbine response. The annular sinusoidal flow was generated through spatial variation of the inlet velocity: the axial inlet velocity

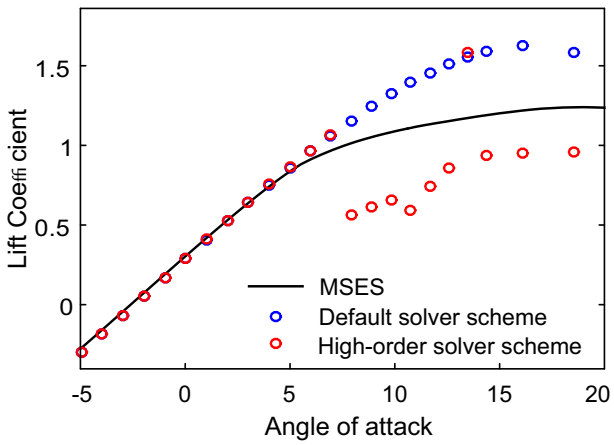


Fig. 8. 2D performance curve of the representative NACA aerofoil, showing MSES results and two characteristics predicted by OpenFOAM, using different solver schemes.

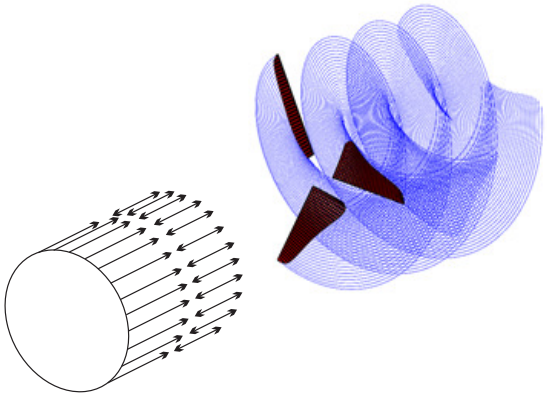

(a) Axially uniform unsteady flow

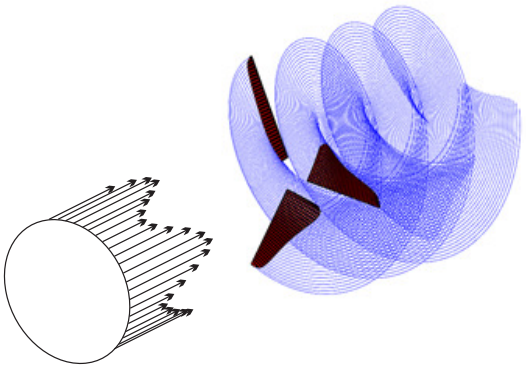

(b) Annular-sinusoidal unsteady flow

Fig. 9. Illustrations of the harmonic unsteady inflow conditions applied to both the vortex lattice models and the URANS simulations.

was set to vary sinusoidally with the annulus angle, with no variation in time (Fig. 9b). This effectively meant that the turbine blades rotated through a series of steady jets, the magnitude of which varied sinusoidally around the annulus.

Unlike the uniform gusts, the annular-sinusoidal gust did not propagate instantaneously, but travelled through the domain with the flow. As such, the sinusoidal gusts required more simulation time, and the gust amplitude diminished gradually due to dissipation (see Fig. 10). All sinusoidal gusts were tested in empty inlet domains prior to simulation, so that the amplitude of the gust at the blade location could be found for a given inlet gust amplitude.

Simulating only a third of the turbine annulus places no restriction on the axially uniform gust, as

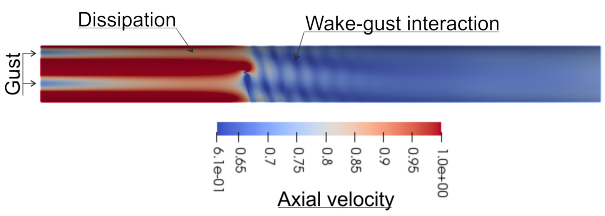


Fig. 10. Contours of axial velocity from URANS simulation, at 85% span radius, with annular-sinusoidal variation of the inflow.

each blade is affected equally and at the same time. The annular-sinusoidal gusts, however, must have an integer number of wavelengths present in the domain to avoid a discontinuity at the periodic boundary. For a third of an annulus the spatial gust distribution must be given by $sin(3\theta n)$, where n is an integer. The maximum value of n considered was 2, as gusts with higher frequencies were found to dissipate excessively by the time they reached the rotor plane and the reduced frequency was unfeasibly large.

In order to study the effects of unsteady flow amplitude on the viscous unsteady response, two different oscillating velocity amplitudes were considered for the uniform gusts: 15% and 7.5% of the steady axial freestream velocity. These gusts correspond to a mid-span angle of attack variation of 3.0° and 1.5°, respectively (the incidence variation at the hub will be larger).

For the uniform gust simulations the Courant number was set to 1000 while the unsteady turbine wake was propagating through the domain. When the unsteady wake reached the domain outlet the Courant number was reduced first to 100 for at least one load cycle, then to 10 for at least two load cycles. For the annular-sinusoidal gusts, the Courant number was kept at 100 while the gust was propagating through the domain, as raising it to 1000 caused the gust to dissipate completely. A Courant number of 10 resulted in a time step that could capture frequencies up to 17,000 Hz, according to the Nyquist criterion. As a comparison, the turbine rotational frequency was 1.8 Hz and the highest gust frequency tested was 10.9 Hz. As such, a Courant number of 10 was sufficient to capture the relevant oscillations in the flow. This assumption was justified by the results, as reducing the Courant number from 100 to 10 did not alter the unsteady load response.

## V. Results

### G. Steady performance

Definitions for all the non-dimensional parameters used in this section can be found in Table II. Fig. 11 shows the steady power and thrust coefficients for the turbine, Cp and Ct, both measured experimentally and predicted by the RANS and the vortex lattice model (VLM). The black line shows the experimentally measured performance. The agreement between the experimental data and the steady RANS simulation (green circles) is good at the rated TSR of 4. The agreement is less good at higher and lower TSR. There are a several potential reasons for this discrepancy. As observed in the previous section and illustrated in Fig. 8, the stall characteristics of the aerofoil are not captured accurately in the CFD simulation. The flow tends to remain attached at higher angles of attack, which leads to over-prediction of the torque at low TSR, as observed in Fig. 11a. Another reason for the discrepancy in the results may be the Reynolds number. In the experiment the TSR was changed by

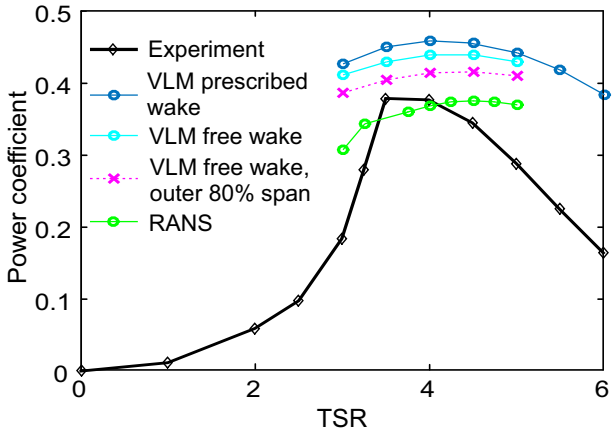


(a) Power coefficient

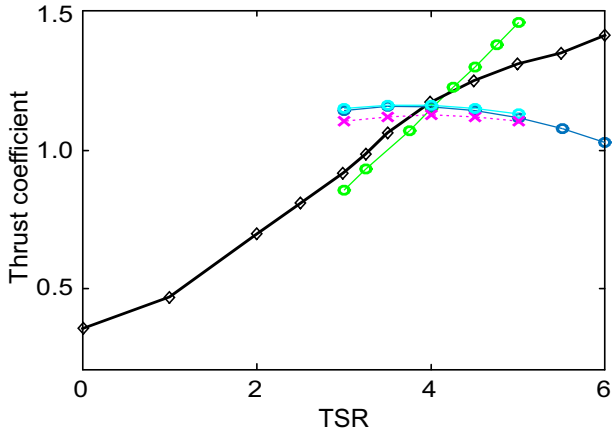


(b) Thrust coefficient

Fig. 11. Steady performance curves of the turbine, as predicted by prescribed-wake VLM, free-wake VLM, and RANS simulations. The results are compared to experimental measurement.

adjusting the turbine rotational speed with constant inlet velocity. In the RANS simulation the TSR was changed by adjusting the inlet flow velocity. This was done to provide representative comparisons to the unsteady gust response, since the gusts are generated by varying the inlet velocity. However, this means that the CFD and experimental tests were done at different Reynolds numbers for off-design TSR, which affects the performance characteristics.

The blue line in Fig. 11 is the performance as predicted by the prescribed-wake VLM, using equation (11) to generate the wake. As such, no wake distortion effects are included. The predicted TSR of peak power is similar to the RANS results, but the magnitude is over-predicted. The light blue lines show instead the steady performance as predicted by the time-stepping VLM using equation (12). Here the wake rollup is included, causing a lowering of the power coefficient due to increased wake damping. The remaining discrepancy can be largely attributed by the inability of the VLM to capture viscous stall. The angle of attack in the hub region is very high, in the order of 20-30 degrees, and so an inviscid model will predict very large lift, while in reality the flow will be separated.

TABLE II
NON-DIMENSIONAL PARAMETERS USED

| Name | Label | Equation |
|---|---|---|
| Torque (Nm) | Q | |
| Thrust (N) | T | |
| Turbine rotation (rad/s) | $\Omega$ | |
| Power coefficient | Cp | $Q\Omega/(0.5\rho U_\infty^3 A)$ |
| Thrust coefficient | Ct | $T/(0.5\rho U_\infty^2 A)$ |
| Gust amplitude | $\eta$ | $\Delta u_{gust}/(2U_\infty)$ |
| Unsteady power coefficient | $Cp/\eta$ | $(Q-\overline{Q})\Omega/(0.5\rho U_\infty^3 A\eta)$ |
| Unsteady thrust coefficient | $Ct/\eta$ | $(T-\overline{T})/(0.5\rho U_\infty^2 A\eta)$ |

The pink line in Fig. 11 shows an estimate of the discrepancy caused by the lack of hub stall in the panel method. It includes only the power and thrust generated over the outermost 80% of the blade span and gives a closer agreement with the RANS results. Neglecting the innermost 20% of the span in the RANS simulation reduces the power coefficient by less than 1%, which does not make a visible change on the power curve. This illustrates that the discrepancy between the vortex lattice method and CFD is largely attributable to the lack of stall in the inviscid code. The low Reynolds number of the CFD and experiments may also contribute to the remaining discrepancy.

The steady thrust coefficient is shown in Fig. 11b. The RANS and VLM simulations do not model the hub, nacelle or support mast and so a correction parameter from Von Mises [33] has been included by modelling these components as cylinders and spheres. With this correction the agreement of the RANS simulation with the experiment is good. The inviscid VLM methods, however, show a different trend from both the RANS simulation and the experiment. This is expected, as the viscous terms will contribute significantly to the thrust, especially at off-design conditions.

### *H. Unsteady loads: time-stepping vortex lattice model*

The results presented in this section show the effect of wake shape on the results from the time-domain VLM. The effects of the two different unsteady flow states - uniform and sinusoidal - are also evaluated. The turbine was first simulated undergoing uniformly oscillating inflow, with gust amplitude of 15% of the mean freestream velocity, at a reduced frequency of 0.35 at the turbine mid-span. The simulation was repeated with each of the wake equations from Section III-C: prescribed convection with the bulk flow (equation (11)), with wake rollup (equation (12)), with distortion of the wake by the unsteady gust (equation (13)) and with both wake rollup and gust distortion (equation (14)). The amplitude of the unsteady response and the mean power coefficient are shown as a bar chart in Fig. 12.

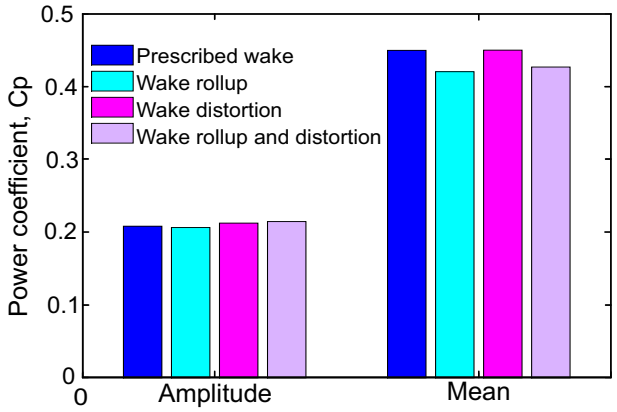


Fig. 12. The unsteady amplitude and mean power coefficient, as predicted by the different time stepping VLM cases, for an axially uniform gust with mid-span reduced frequency 0.35.

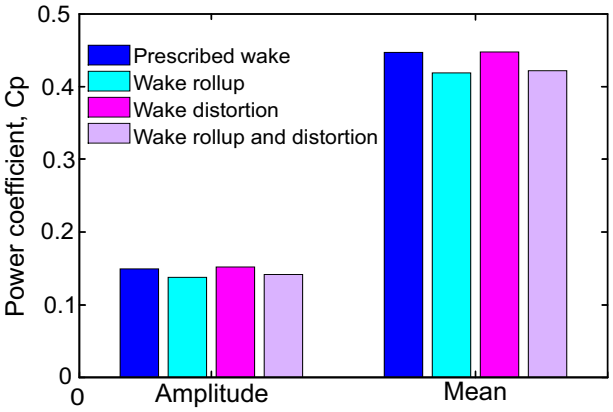


Fig. 13. The unsetady amplitude and mean power coefficient, as predicted by the different time stepping VLM cases, for an annular-sinusoidal gust with mid-span reduced frequency 1.1.

The dark blue bars in Fig. 12 represent the 'baseline' prescribed-wake case. Comparing these to the light blue bars representing the inclusion of wake rollup, the effect of wake rollup is primarily a reduction in the mean power coefficient. This is in line with the finding in Section V-A where the inclusion of wake rollup in steady state simulations was found to reduce the power coefficient. Comparing the dark blue to the bright pink bars, representing wake distortion by the unsteady gust, the distortion increases the unsteady response amplitude without affecting the mean power coefficient. The changes to the unsteady amplitude are however small overall, differing only by a few per cent.

Fig. 13 shows the variation of power coefficient when the turbine undergoes sinusoidally varying inflow, as illustrated in Fig. 9b. The unsteady flow amplitude is again 15% of the mean freestream velocity, and the mid-span reduced frequency is 1.1. The results differ from the uniform oscillation cases, in that wake rollup effects (light blue) have a significant impact on the unsteady load amplitude compared to the prescribed wake case (dark blue), reducing it by almost 8%. The gust distortion effects (bright pink) are relatively modest. In both Fig. 12 and Fig. 13 the wake rollup and gust distortion effect adds up in an approximately linear way. Not shown in Figs. 12 and 13 are the phase of the unsteady response. This was found to change with different wake models for the uniform gust, but not for the sinusoidal gust.

There are a few possible reasons as to why the results for the two unsteady flow cases differ. The two physical effects responsible for inviscid unsteady loading are the added mass and the downwash caused by the unsteady wake. If, for a particular unsteady flow case, the wake is the dominant factor of the two, changes to the wake should have a relatively larger effect on the load response. This may be the case for the case in Fig. 13. However, parameters such as the unsteady flow frequency and amplitude will also affect whether the wake downwash or added mass are dominant, so it is not simply a matter of the 'shape' of the unsteady flow.

The frequency-domain VLM with the wake shape corrected for steady flow (as described in section III-D) will be compared to the prescribed-wake VLM and URANS results in the next section. While this correction will not give answers equivalent to the time-domain VLM, it will provide an estimate of the effects of wake rollup on the unsteady response for a range of unsteady flow frequencies. Gust distortion effects, on the other hand, cannot be modelled in the frequency-domain because the correction would need to be applied at every time step for each gust. The fact that gust distortion has been shown to have only a small effect on the unsteady response (see Figs. 12 and 13) means that neglecting it is unlikely to cause large errors.

### *I. Unsteady loads: accuracy of frequency-domain inviscid modelling in 2D and 3D*

The results presented in this section concern the frequency-domain VLM, both with the original prescribed-wake method and with the steady wake correction method outlined in section III-D. The results are compared to a series of URANS simulations described in section IV. The ability of 3D inviscid modelling to predict the unsteady loading of a tidal turbine geometry is thus evaluated. The results are also compared to predictions by 2D strip theory.

The results in this section are shown in terms of unsteady normalised power and thrust coefficients, which were found by Sequeira [27] to be the appropriate way of normalising the unsteady flow response of turbine aerofoils. The definition (given in Table II) is the unsteady variation in power or thrust coefficient, normalised by the unsteady flow amplitude (which is itself expressed as a fraction of the mean axial flow).

Fig. 14 shows a single load cycle of the turbine, for two different unsteady flow conditions. Fig. 14a shows the response to uniform axial oscillation of the inflow, while Fig. 14b shows the response to an annular-sinusoidal inflow. The reduced frequency at

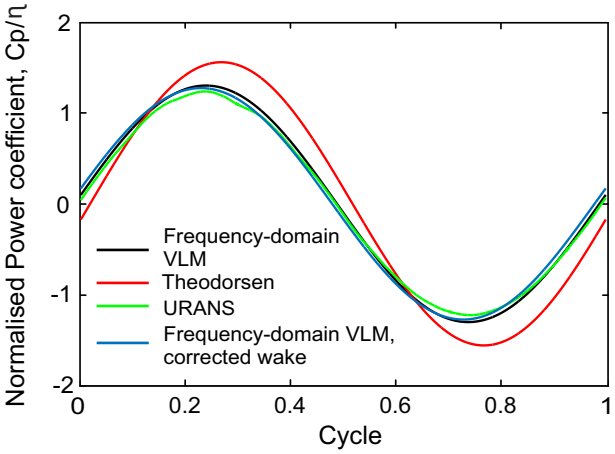


(a) Mid-span reduced frequency 0.16, uniform oscillation flow

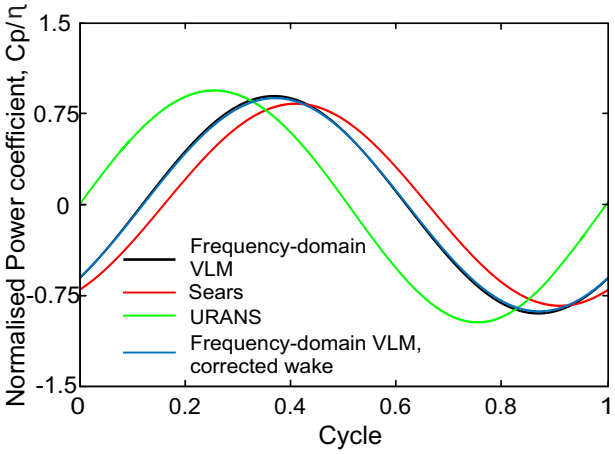


(b) Mid-span reduced frequency 1.1, sinusoidal inlet flow

Fig. 14. Normalised power coefficient during a single load cycle, as predicted by URANS, frequency-domain VLM, and 2D functions from classical aerofoil theory.

mid span is 0.16 in the former case, and 1.1 in the latter.

The unsteady load predictions are shown from the original VLM, the wake-corrected VLM, the URANS simulation, and classical 2D aerofoil theory. The Theodorsen function was used for the uniform gust, and the Sears function for the sinusoidal inflow. The URANS result in Fig. 14a (green line) is in fact not a perfect sinusoid, indicating nonlinear viscous effects. The URANS results in Fig. 14b have a smoother response curve. In general, the URANS response showed more nonlinear effects at low unsteady flow frequencies. This was the case for both the gust amplitudes tested (7.5 and 15% of the mean axial flow), meaning that for this particular set of parameters the flow frequency was the dominating factor in determining nonlinear viscous effects, as opposed to the amplitude of the unsteady gust.

Fig. 14a shows that the 2D prediction (red line) significantly over-predicts the unsteady load amplitude, and also the phase lag. The results from the original VLM (black line) and the corrected VLM (blue line) give similar results for this gust frequency, and correspond well to the load amplitude predicted by URANS simulation. The phase is also quite well predicted by the 3D models. Fig. 14b shows that the original and corrected VLM give virtually the same result, and all three inviscid models slightly under-predict the load amplitude. The phase lag is also severely over-predicted by both the 2D and the 3D inviscid models.

In order to see the trends predicted across a range of unsteady flow frequencies, Figs. 15 to 18 show the unsteady response separated into the amplitude and phase, plotted against the mid-span reduced frequency. The amplitude is defined as the peak-to-peak normalised power or thrust coefficient. In the URANS results the phase varies slightly over the load cycle, and so the phases shown in Figs. 15 to 18 are therefore averaged over one load cycle.

Fig. 15 and Fig. 16 show the unsteady amplitude and phase of the turbine load response to axially uniform oscillating inflow. Predictions from the URANS, original VLM and corrected VLM are shown, along with the Theodorsen function. Fig. 15 shows the results in terms of the normalised power coefficient. The VLM prediction corresponds remarkably well to the URANS results, with the trend being well matched to the prediction by the 3D models. The 2D model, by comparison, starts out by over-predicting the amplitude, and then under-predicts it in the intermediate frequency range. The wake correction to the VLM has a significant impact on the load response, but does not necessarily improve the correspondence to the URANS results. Fig. 15b shows a similar trend in the phase. The deviation between 2D and 3D response prediction is significant, with the phase responses following completely different trends and the 3D model offering better agreement with the URANS results.

Fig. 16 shows the turbine load response in terms of the normalised thrust coefficient. While there is still fairly good agreement with the 3D VLM predictions, the amplitude is under-predicted compared to URANS results at lower gust frequencies. This is generally true also for the 2D prediction, which only gives a conservative estimate in the case of the URANS data point at the lowest frequency. The addition of the steady wake correction to the VLM improves the agreement slightly. The agreement in the phase prediction (Fig. 16b) is less good, however it should again be noted that it was difficult to define the phase from the URANS results.

Fig. 16 shows that the thrust coefficient approaches the 2D characteristic with increasing reduced frequency. Fig. 15, however, shows the power coefficient deviating significantly from the 2D function throughout the frequency range. This can be explained by considering the characteristics of unsteady flow in 3D. In a previous study by the authors [25] 3D effects were found to dominate near the blade tips; the local unsteady lift was found to approach the 2D characteristic, except for near the blade tips, where it

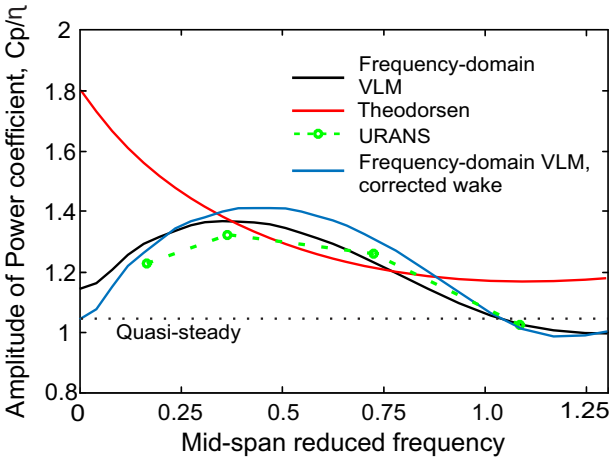


(a) Unsteady amplitude of normalised power coefficient

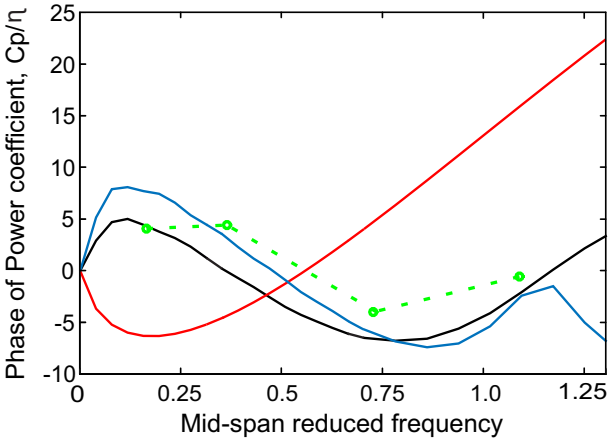


(b) Unsteady phase of power coefficient

Fig. 15. Normalised power coefficient for a range of gust frequencies. The results are for uniformly oscillating inflow.

remained significantly 3D throughout. This suggested that for tidal turbines 3D effects would have the most significant consequences for unsteady torque and bending moment, since these are mainly generated near the blade tips. Thrust, on the other hand, would approach 2D behaviour at high reduced frequencies. This is what we see in Figs. 15 and 16.

Fig. 17 and Fig. 18 show the amplitude and phase response to inflow varying sinusoidally around the turbine annulus. The URANS and 3D VLM results are compared to predictions from the Sears function. In this case, due to the limitations on the simulation of sinusoidal inflow mentioned in section IV, only two inflow frequencies were simulated in URANS. Fig. 17 shows the unsteady response in terms of the normalised power coefficient. The unsteady amplitude is quite well predicted by the 3D VLM models compared to the URANS results. The phase however, as also noted in relation to Fig. 14b, is not well predicted at all. The results also show that the steady wake correction does not make a big difference to the response characteristic, unlike in the case of the axially uniform oscillatory inflow in Figs. 15 and 16.

Fig. 17 shows the amplitude and phase response in terms of the normalised power coefficient, and Fig. 18 the normalised thrust coefficient. Again, the unsteady amplitude compares well between the URANS and VLM results. The steady wake VLM correction does not significantly affect the results, other than slightly amplifying the returning wake effects. As mentioned in the discussion of Figs. 15 and 16, we expect the thrust to approach the 2D characteristic at high reduced frequencies, but not the torque. This is because 3D effects are confined to the tip region at high frequencies. Notably, however, in Figs. 17 and 18 the trend is the opposite. The unsteady power coefficient in Fig. 17 appears to approach the 2D characteristic, while the thrust coefficient in 18 does not.

A possible explanation for the break from the expected trend in Figs. 17 and 18 could be that the effect of the unsteady wake is substantially smaller for the annular-sinusoidal gust, compared to the axially uniform gust. Recall that inviscid unsteady response consists of added mass forces and aerodynamic damping by the unsteady wake. For a sinusoidal gust the added mass will be relatively small, and if the wake damping is also small the response will be approximately quasi-steady. This is in fact what we see for the thrust coefficient, in Fig. 18. For reduced frequency less than 1.0 the characteristic oscillates

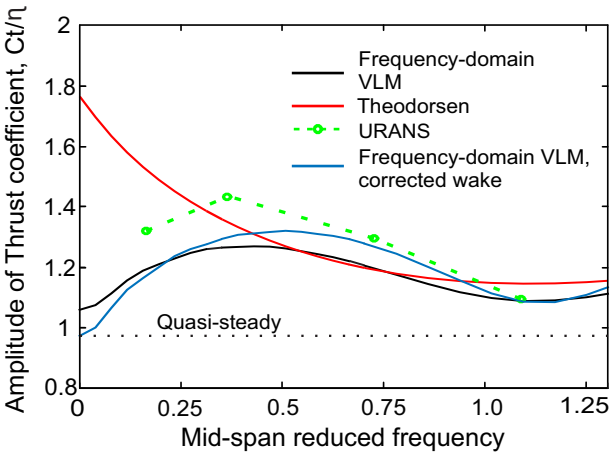


(a) Unsteady amplitude of normalised thrust coefficient

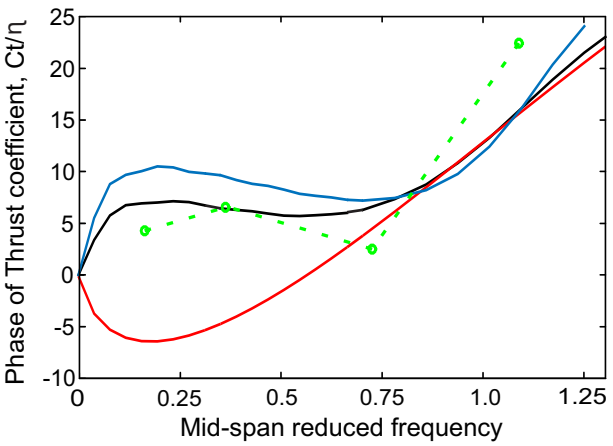


(b) Unsteady phase of thrust coefficient

Fig. 16. Normalised thrust coefficient for a range of gust frequencies. The results are for uniformly oscillating inflow.

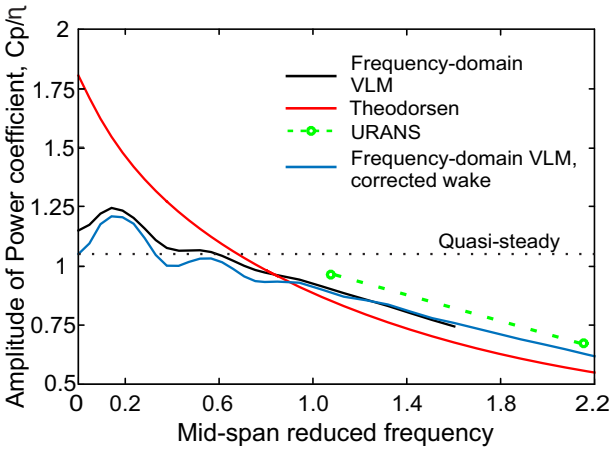


(a) Unsteady amplitude of normalised power coefficient

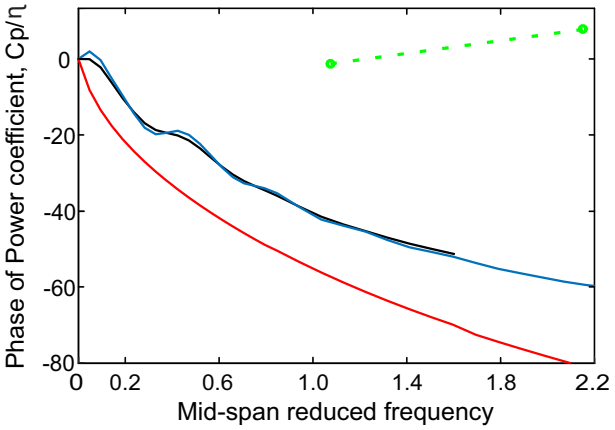


(b) Unsteady phase of power coefficient

Fig. 17. Normalised power coefficient for a range of gust frequencies. The results are for annular-sinusoidal inflow.

around approximately the quasi-steady value (the oscillations being due to returning wake effects). The unsteady power coefficient (Fig. 17) is more affected by 3D wake damping than the thrust, because it is primarily dependent on the load near the blade tips. As such, the unsteady amplitude of the power coefficient is less than quasi-steady throughout a majority of the frequency range, resulting from the aerodynamic damping by the 3D wake. However, its apparent similarity to the 2D characteristic at high frequencies is likely to be a coincidence, as the physical origin of the wake damping is different for the 2D and 3D models.

From the results presented in this section we can conclude that the 3D inviscid VLM provides good predictions of the unsteady load response. The steady wake correction provides a slight improvement of the model, but by far the most significant is the improvement by using a 3D model instead of 2D functions. The 2D characteristic has been shown to be unable to predict the unsteady load response. The inadequacy of the 2D model is particularly stark in the case of blade torque. This is due to the fact that 3D effects are concentrated at the tips of the blade, which contribute more strongly than the inboard sections to torque. Bending moment calculations are not included here, but these would show a similar effect.

## VI. Discussion and Conclusions

A previous study by the authors [25] identified key factors that determined the degree to which 3D geometry effects impact unsteady flow response. 3D effects were found to be most significant at low reduced frequency, low aspect ratio, and near blade tips. The objective of this study has been to estimate the 3D effects of wake rollup and gust distortion of the wake, and to quantify viscous effects. One of the end goals of this study is to illustrate the differences between 2D and 3D unsteady flow response, and to show how 3D unsteady effects can impact turbine lifetime predictions.

Fig. 15 and Fig. 16 - the turbine load response to a uniform gust - appear to agree with the previous study. In the case of thrust predictions (Fig. 16), 3D effects are most significant at low reduced frequencies, and the characteristic approaches the 2D curve at higher frequencies. The unsteady blade bending moment, shown in terms of the unsteady power coefficient in Fig. 15, deviates more strongly from the 2D characteristic. This is also expected, as 3D effects are most significant near blade tips and remain large for all frequencies in that region. Since the tip section of the blade contributes the most to the bending moment, the 3D unsteady power coefficient does not

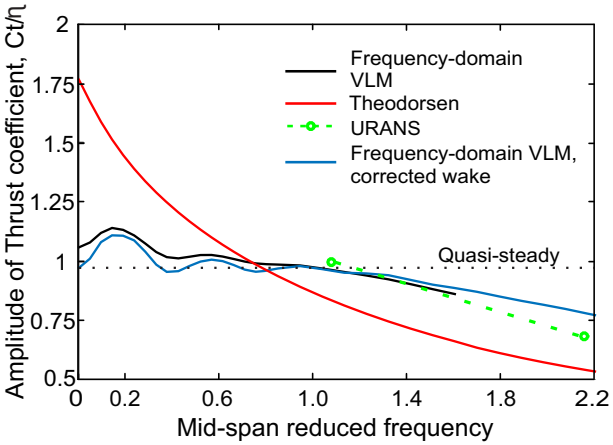


(a) Unsteady amplitude of normalised thrust coefficient

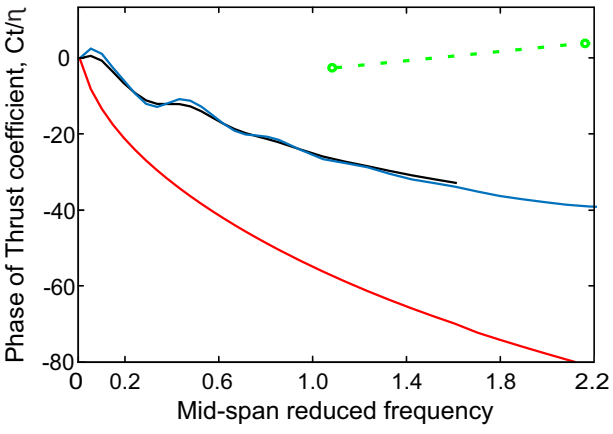


(b) Unsteady phase of thrust coefficient

Fig. 18. Normalised thrust coefficient for a range of gust frequencies. The results are for annular-sinusoidal inflow.

approach the 2D prediction even at high frequencies.

Fig. 17 and Fig. 18 - the response to a sinusoidal gust - show different trends, with the torque approaching the 2D characteristic at high frequencies and the thrust deviating from it. This was explained by the thrust response being nearly quasi-steady throughout the frequency range, having neither significant added mass nor unsteady wake effects. The torque is, by comparison, more affected by the 3D wake. Because of this its unsteady amplitude is less than quasi-steady for most of the frequency range, due to the increased aerodynamic damping by the 3D wake.

Comparing the 2D and 3D predictions of load amplitude in Figs. 15 to 18, some important differences can be seen. The 3D model shows that the peak load amplitude is not the quasi-steady value (which is what the 2D models predict), but occurs in the reduced frequency range 0.4-0.6 for axially uniform gusts, and in the range 0.1-0.3 for annular-sinusoidal gusts. In the case of the axially uniform gusts, the load amplitude is also under-predicted by the 2D function in this range. As such, neither the quasi-steady response nor the 2D functions can be assumed to give conservative estimates of unsteady loading.

The 3D unsteady wake has been shown to drive much of the unsteady response [25]. It is important to note the implication of this finding for the validity of load estimates based on 2D models. In BEMT modelling the performance of a turbine is evaluated at individual 2D blade sections, and corrections are applied to the 2D lift coefficient to account for the steady-flow downwash by the 3D wake. If these quasi-steady corrections are applied to an unsteady 2D lift characteristic, rather than accounting for an unsteady 3D wake, the load amplitude will be severely under-predicted. To illustrate this, Fig. 19 shows the unsteady load response of the turbine for axially oscillating inflow, in terms of the amplitude of the unsteady power coefficient. The 2D amplitude predicted by the Theodorsen function (red line) and the 3D amplitude from the VLM (black line) are the same as in Fig. 15. The red dashed line represents the Theodorsen function corrected for the quasi-steady 3D wake downwash. At reduced frequency 0.5, this correction under-predicts the unsteady load amplitude by over 60% compared to the 3D response. This discrepancy illustrates the hazard in assuming that 3D wake effects are quasi-steady.

The trends predicted by the 3D frequency-domain VLM corresponded well with the URANS simulations. The time-domain VLM showed that including wake rollup effects primarily improved the steady flow results, and that distortion of the wake by the gust had minimal effect on the unsteady load. The prescribed wake used in the frequency-domain VLM can be corrected to account for wake rollup, but wake distortion cannot be corrected for. Including wake rollup effects in the frequency-domain VLM increased the returning-

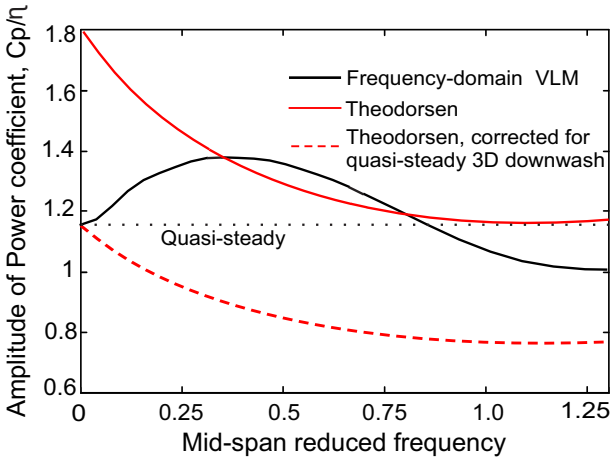


Fig. 19. Unsteady load response, as predicted by the 2D Theodorsen function, 3D VLM, and the Theodorsen function corrected for quasi-steady 3D wake downwash.

wake effects, and gave marginally improved agreement with the URANS results. The speed of the frequency domain tool more than compensates for the small loss of accuracy due to missing the distortion term. As such, this study shows that the inviscid vortex lattice model in 3D is accurate for first order prediction of unsteady turbine loads, and is a suitable tool for tidal turbine design.

## Acknowledgement

The authors would like to thank the Engineering and Physical Sciences Research Council (EPSRC) for providing the funding necessary to complete this research. This includes a Tier-2 capital grant (EP/P020259/1) for high performance computing services, and a Doctoral Training Award PhD Studentship. We would also like to thank Prof. Luca Di Mare for his support in developing the low-order models used in this work, and Dr. James McNaughton for his advice on CFD simulations.

## References

[1] T. H. E. Clark, "Turbulence in Marine Environments (TiME): A framework for understanding turbulence and its effects on tidal devices," *Proceedings of the 11th European Wave and Tidal Energy Conference*, 2015.
[2] A. Winter, "Differences in fundamental design drivers for wind and tidal turbines," *Proceedings of IEEE OCEANS*, 2011.
[3] C. L. Sequeira and R. J. Miller, "Unsteady Gust Response of Tidal Stream Turbines," *Proceedings of the IEEE/MTS OCEANS*, 2014.
[4] T. Burton, D. Sharpe, N. Jenkins, and E. Bossanyi, "Wind Energy Handbook," *John Wiley & Sons*, 2001.
[5] E. Bossanyi, "GH Tidal Bladed Theory Manual," 2007.
[6] J. G. Leishman, "Principles of Helicopter Aerodynamics," *Cambridge University Press*, vol. Chapter 8, 2006.
[7] T. Theodorsen, "General theory of aerodynamic instability and the mechanism of flutter," *NACA Techical Report no. 496*, 1935.
[8] W. Sears, "A Systematic Presentation of the Theory of Thin Aerofoils in Non-Uniform Motion," Ph.D. dissertation, California Institute of Technology, 1938.
[9] D. A. Peters, D. D. Boyd, and C. J. He, "FiniteState InducedFlow Model for Rotors in Hover and Forward Flight," *Journal of the American Helicopter Society*, 1989.
[10] A. Suzuki and A. C. Hansen, "Generalised Dynamic Wake Model for YawDyn," *AIAA Journal*, 1999.
[11] M. Robinson, R. Galbraith, D. Shipley, and M. Miller, "Unsteady Aerodynamics of Wind Turbines," *33rd AIAA Aerospace Sciences Meeting and Exhibit*, 1995.

[12] G. Scarlett, B. Sellar, T. van den Bremer, and I. Viola, "Unsteady Hydrodynamics of a Full-Scale Tidal Turbine," *7th European Conference on Computational Fluid Dynamics (ECFD 7)*, 2018.
[13] J. Leishman, "Challenges in Modelling the Unsteady Aerodynamics of Wind Turbines," *NACA Techical Report no. 496*, 2002.
[14] A. M. Young, J. R. Farman, and R. J. Miller, "Load alleviation technology for extending life in tidal turbines," *Progress in Renewable Energies Offshore-Proceedings of 2nd International Conference on Renewable Energies Offshore, RENEW*, 2016.
[15] M. A. Holst, O. G. Dahlhaug, and C. Faudot, "CFD Analysis of Wave-Induced Loads on Tidal Turbine Blades," *IEEE Journal of Ocean Engineering*, 2010.
[16] I. A. Milne, A. H. Day, R. N. Sharma, and R. G. J. Flay, "Blade loads on tidal turbines in planar oscillatory flow," *Ocean Engineering*, 2013.
[17] D. McNae, "Unsteady Hydrodynamics of Tidal Stream Turbines," Ph.D. dissertation, Imperial College London, 2013.
[18] J. I. Whelan, "A fluid dynamic study of free-surface proximity and inertia effects on tidal turbines," Ph.D. dissertation, Imperial College London, 1987.
[19] S. A. Kinnas and C. Hsin, "Boundary Element Method for the Analysis of the Unsteady Flow Around Extreme Propeller Geometries," *AIAA Journal*, 1992.
[20] M. Namba and K. Toshimitsu, "Double Linearisation Theory of Three-Dimensional Cascades With Vibrating Blades Under Spanwise-Nonuniform Mean Loading, I: Subsonic Flow," *Journal of Sound and Vibration*, 1991.
[21] J. Schulten, "Sound Generated by Rotor Wakes Interacting with a Leaned Vane Stator," *AIAA Journal*, 1982.
[22] K. C. Hall and C. B. Lorence, "Calculation of Three-Dimensional Unsteady Flows in Turbomachinery Using the Linearized Harmonic Euler Equations," *ASME*, 1992.
[23] D. Prasad and J. M. Verdon, "A Three-Dimensional Linearized Euler Analysis of Classical Wake/Stator Interactions: Validation and Unsteady Response Predictions," *International Journal of Aeroacoustics*, 2002.
[24] V. Golubev, H. Atassi, and A. Lipatov, "3-D unsteady effects in annular cascades with swirl and comparison with 2-D strip theory," *3rd AIAA/CEAS Aeroacoustics Conference*, 1997.
[25] A. S. M. Smyth, A. M. Young, and L. Di Mare, "The Effect of 3D Geometry on Unsteady Gust Response, Using a Vortex Lattice Model," *AIAA SciTech*, 2019.
[26] R. G. Loewy, "A two-dimensional approximation to the unsteady aerodynamics of rotary wings," *Journal of the Aeronautical Sciences*, 1957.
[27] C. L. Sequeira, "Hydrodynamics of Tidal Stream Turbines," Ph.D. dissertation, Cambridge University, 2014.
[28] J. Katz and A. Plotkin, "Low-Speed Aerodynamics," *Cambridge University Press*, 2001.
[29] F. X. Caradonna and C. Tung, "Experimental and Analytical Studies of a Model Helicopter Rotor in Hover," *NASA Technical Memorandum 81232*, 1981.
[30] J. R. Farman, "Wireless RF Telemetry for Rotating Frame Data Acquisition and Control," *XXIII Biannual Symposium on Measuring Techniques in Turbomachinery*, 2016.
[31] C. J. Greenshields, "OpenFOAM User Guide, version 6," 2018.
[32] M. Drela, *A users guide to MSES 3.05.* MIT Department of Aeronautics and Astronautics, 2007.
[33] R. von Mises, *Theory of Flight*. New York: Dover Publications, Inc., 1959.